3376 *Macromolecules* **2010**, *43*, 3376–3382
DOI: 10.1021/ma9025509

Macromolecules
ARTICLE

Crystallization in the Binary Blends of Crystalline−Amorphous Diblock Copolymers Bearing Chemically Different Crystalline Block

Che-Yi Chu,[†] Hsin-Lung Chen,*[,†] Ming-Siao Hsiao,*[,‡,∥] Jean-Hong Chen,[§] and Bhanu Nandan[†,⊥]

[†]*Department of Chemical Engineering, National Tsing Hua University, Hsin-Chu 30013, Taiwan,* [‡]*Material and Chemical Research Laboratories, Industrial Technology Research Institute, Hsin-Chu 300, Taiwan, and* [§]*Department of Polymer Materials, Kun Shan University, Tainan Hsien 71003, Taiwan.* [∥] *Present address: Department of Polymer Chemistry, Graduate School of Engineering, Kyoto University, Nishikyo-ku, Kyoto 616-8510, Japan.* [⊥] *Present address: Leibniz Institute of Polymer Research Dresden, Hohe Strasse 6, 01069 Dresden, Germany.*

Received November 19, 2009; Revised Manuscript Received February 8, 2010

ABSTRACT: The crystallization behavior of the blends of two crystalline−amorphous diblock copolymers bearing chemically different crystalline block has been studied. A series of lamellae-forming blends of a polystyrene-*block*-poly(ethylene oxide) (SEO) with shorter block lengths and a polystyrene-*block*-poly(L-lactide) (SLLA) with longer block lengths were prepared. Over the composition range investigated, the PS blocks from these two copolymers were found to mix intimately in the PS lamellar microdomains in the melt; moreover, the PEO and PLLA blocks also formed a miscible mixture in their domains. Because of the constraint imposed by the junction points localized at the lamellar interface and the nanoscale confinement effect, the crystallization behavior of PEO and PLLA blocks within the lamellar microdomains was found to deviate from that in the corresponding homopolymer blends. In the SLLA-rich blends, the junction point constraint coupled with the poor chain mobility at low crystallization temperature ($\leq \sim$45 °C) hampered the relatively long-range transport of PLLA segments for crystal growth. In this case, a local demixing between a fraction of PEO and PLLA chains took place, yielding the PLLA crystalline domains in which the PLLA crystalline stems were intervened by the PEO chains. This crystalline species gave rise to a relatively broad peak at $2\theta = 15.92°$ in the wide-angle X-ray scattering profile and displayed a much lower melting point of ca. 100 °C compared to that of the typical α-form crystal of PLLA. It was suggested that the inserted PEO chains served as the molecular defects which induced an expansion of the *a*-axis and *b*-axis of the α-form PLLA unit cell and lowered the crystal melting point due to introduction of defect free energy.

Introduction

Crystalline−amorphous (C−A) diblock copolymers have received significant attention. The majority of interests involve the use of this type of copolymer as a model for studying the crystallization behavior of chain molecules under nanoscale confinement, where lamellar, cylindrical, and spherical microdomains offer the confinement in one, two, and three dimensions, respectively.[1−5] Such a spatial confinement was found to impose dramatic effects on the crystal orientation and the crystallization kinetics.[3,6−11] Another interesting aspect of C−A diblock is the interplay between the driving forces of microhpase separation and crystallization that leads to a perturbation of the microphase-separated morphology established in the melt state. Recent studies have revealed that the glass transition temperature (T_g) of the amorphous block and the segregation strength play decisive roles governing the ability of crystallization to perturb the melt mesophase.[12−14] As a result, it is feasible to design a variety of morphology in C−A diblocks by balancing the thermodynamic and kinetic parameters associated with microphase separation and crystallization.

The present study concerns the crystallization behavior of a more complex system, namely, the blends of two C−A diblock copolymers bearing chemically identical A block. This type of blend can be classified into the following two systems: (1) C_n-*b*-A_m/C_l-*b*-A_k blend (with the subscripts denoting the block length), where the two diblocks forming the blend are chemically identical but have different block lengths; (2) C_n-*b*-A_m/C_l'-*b*-A_k blend, where the crystalline blocks (C_n and C_l') are chemically different.

The phase behavior of the first system in the melt state has been well studied both experimentally and theoretically.[15−21] Recent investigations of the blends of a short symmetric diblock and a long symmetric or slightly asymmetric diblock indicated that the two types of blocks could mix in their respective microdomains, with the short diblock acting as the cosurfactant for the long diblock copolymers. When considering the crystallization behavior of C_n-*b*-A_m/C_l-*b*-A_k blend with C_n and C_l block and A_m and A_k blocks mixing intimately in their respective microdomains in the melt, one question which arises naturally is whether C_n and C_m blocks would cocrystallize or phase segregate upon crystallization? Cocrystallization is of course more likely if the crystallization temperature (T_c) is lower than the T_g of the amorphous block because the immobility of the junction points at the interface may restrict the phase segregation of the two crystalline bocks upon crystallization. Our previous study of the blends of two polybutadiene-*block*-poly(ethylene oxide)s (PB-*b*-PEO) showed that even when T_c was well above the T_g of PB block, the PEO blocks of different chain lengths in the blends could cocrystallize over a broad range of undercooling.[22] The cocrystallization was proposed to be a thermodynamic requirement for

*To whom correspondence should be addressed. E-mail: hlchen@che.nthu.edu.tw (H.-L.C.); victorhsiao0523@gmail.com (M.-S.H.).

 Published on Web 03/19/2010

attaining a lower interfacial energy and a higher conformational entropy of the longer PB blocks in the system.

In the present study, we explore the crystallization behavior of the second type of blend system, C_n-*b*-A_m/C_l'-*b*-A_k, formed by a polystyrene-*block*-poly(ethylene oxide) (PS-*b*-PEO, abbreviated further as SEO) and a polystyrene-*block*-poly(L-lactide) (PS-*b*-PLLA, abbreviated further as SLLA), with PEO and PLLA being the crystalline blocks. It has been shown previously that the binary blends of PEO and PLLA homopolymers with low to moderate molecular weights ($M_{PEO} < 10^5$ g/mol) were miscible in the melt but they did not cocrystallize.[23−28] A series of recent studies by Mao and Hillmyer have revealed that the binary blends of SEO and PS-*b*-poly(DL-lactide) (in which the racemic PLA block cannot crystallize) did not exhibit macrophase separation; instead, PEO and PLA blocks formed a single composite microdomains confined within a common PS matrix.[29−31] The crystallizability of PEO block was further found to be suppressed significantly due to the nanoconfinement effect.

Here we mix a shorter symmetric SEO with a longer slightly asymmetric SLLA to yield a series of lamellae-forming blends with different SLLA contents. In the melt state, the binary blends contain PS lamellae formed by the mixture of the PS blocks from the two copolymers and PEO/PLLA lamellae in which the PEO and PLLA blocks mix intimately. The crystallization of PEO and PLLA blocks are effectively confined within the PEO/PLLA microdomains over a broad range of T_c; in this case, it would be of interest to examine whether the two chemically different blocks can cocrystallize. Even if the two crystalline blocks do not cocrystallize, it will still be of interest to explore how the localizations of junction points coupled with the intimate mixing under spatial confinement would affect the crystallization behavior of PLLA and PEO blocks. It will be shown here that cocrystallization of PEO and PLLA blocks did not take place over the composition and crystallization conditions studied. The crystallization behavior of PLLA was however significantly modified in the copolymer blends compared to that in the corresponding homopolymer blends, where the crystallization of PLLA at low T_c in SLLA-rich blends led to the formation of the PLLA crystallites in which the PLLA crystalline stems were intervened by the PEO chains. The orientation of PLLA crystallites in the lamellar microdomains of a SLLA-rich blend will also be revealed.

Experimental Section

Materials and Sample Preparation. PS-*b*-PEO (M_{PS} = 9500, M_{PEO} = 9500, PDI = 1.07) and PS-*b*-PLLA (M_{PS} = 21 000, M_{PLLA} = 19 500, PDI = 1.11) were purchased from Polymer Source, Inc. The volume fractions of PLLA blocks in these two samples were 0.49 and 0.44, respectively, at room temperature. For the blend preparation, the two copolymers with desired weight ratios were dissolved in chloroform to yield 3 wt % solutions. The solutions were subsequently cast on the Petri dishes, and the blend films were obtained after evaporating most solvent slowly at room temperature. The films were then further dried in vacuum at 60 °C for 4 h.

The crystalline samples of SEO, SLLA, and their blends were basically prepared by isothermal crystallizations at the desired T_cs for 48 h. The samples were first annealed at 190 °C for 10 min to erase previous crystallization history followed by rapid cooling (> 100 °C/min) to T_c.

Small-Angle X-ray Scattering (SAXS) Measurement. The morphology of the diblocks and their blends in the melt state was probed by a Bruker NANOSTAR SAXS apparatus. The SAXS instrument was equipped with a 3.0 kW X-ray generator operated at 40 kV × 35 mA and a two-dimensional position-sensitive proportional counter. The Cu Kα line (λ = 0.154 nm) was used. For the melt structure characterization, the samples were first equilibrated at 190 °C for 30 min followed by data acquisition for 30 min. The scattering intensity profile was output as the plot of the scattering intensity (I) vs the scattering vector, $q = (4\pi/\lambda)\sin(\theta/2)$ (θ = scattering angle). The SAXS profiles were corrected for the absorption, the air scattering, and the background arising from thermal diffuse scattering (TDS).

Temperature-Dependent Wide-Angle X-ray Scattering (WAXS) Measurement. The WAXS experiment was conducted at the wiggler beamline BL17A1 of the National Synchrotron Radiation Research Center (NSRRC), Taiwan. A triangular bent Si (111) single crystal was used to obtain a monochromatic beam of wavelength λ = 1.54 Å. 2-D diffraction patterns were collected using imaging plates (Fuji BAS III, area = 20 × 40 cm^2) having 100 μm pixel resolution. For the temperature dependence experiment, the WAXS profiles of a given sample were collected at various temperatures *in situ* in a heating cycle. The sample was held at the prescribed temperature for 5 min followed by data acquisition for another 5 min for each measurement. The accuracy of temperature control was ±0.5 °C.

Differential Scanning Calorimetry (DSC) Measurement. The melting behavior of SEO/SLLA blends was studied by a TA Instruments 2000 DSC equipped with the RCS cooling system. The DSC heating scans of the samples isothermally crystallized at the prescribed T_cs for 48 h were recorded from −5 to 190 °C at the heating rate of 20 °C/min.

Large-Amplitude Oscillatory Shear (LAOS) Experiment. To study the crystal orientation in SEO/SLLA 20/80 blend, a Linkam CSS450 temperature-controlled shear system was used to prepare the oriented sample by large-amplitude oscillatory shear (LAOS). The sample was preshaped into thin disks of suitable thickness and diameter and held in the gap between the two glass windows. Subsequently, they were pressed between the two plates at 190 °C and sheared for 1 h using an amplitude oscillatory step of the bottom plate. The shear amplitude and the frequency were 80% and 0.2 Hz, respectively.

Results and Discussion

Miscibility and Melt Morphology of SEO/SLLA Blends. Figure 1a shows the SAXS profiles of SEO, SLLA, and SEO/SLLA blends collected in the melt state (T = 190 °C). The solid curves represent the fits of the experimental data by the paracrystalline model of lamellar structure considering polydispersity of lamellar thickness, limited grain size, and lattice distortion by thermal fluctuations.[32] Neat SEO displayed a lamellar morphology as evidenced by integral position ratio of the scattering peaks and the good fit of the experimental data by the paracrystalline model. Neat SLLA was found to exhibit a hexagonally packed cylinder morphology as the scattering pattern showed a series of peaks with the position ratios of $1:3^{1/2}:4^{1/2}:7^{1/2}$. Considering that the χN value (calculated using $\chi(T) = 96.6/T - 0.091$ as reported by Hillmyer et al.) and the volume fraction of PLLA block (f_{PLLA}) was 39.7 and 0.43 at 190 °C, respectively, the formation of hexagonal phase was indeed consistent with the phase diagram of PS-*b*-PLA established by Hillmyer et al.[33]

A major issue here is the miscibility of the PS blocks from the two copolymers and also that between PEO and PLLA blocks in their respective microdomains in the melt state. As shown in Figure 1a, the blends of SEO and SLLA displayed lamellar morphology over the composition range investigated, as evidenced by the multiple scattering peaks showing integral position ratios as well as the satisfactory fits by the paracrystalline lamellar model. The formation of lamellar morphology by the blends was indeed expected if the constituting blocks from the two copolymers were miscible in their respective domains because the overall volume fractions of PS component in the blends ranged from 0.52 to 0.54. Figure 1b plots the interlamellar distance (d) and the area per junction point at the lamellar interface (Σ) as a

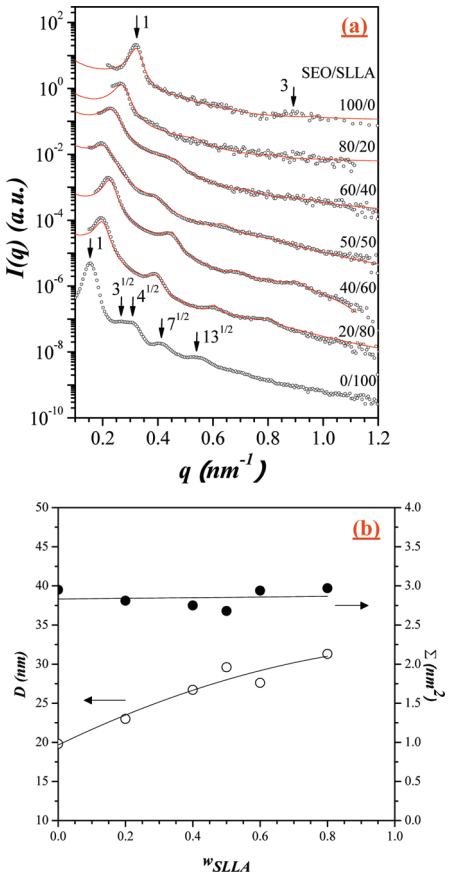

Figure 1. (a) SAXS profiles of SEO, SLLA, and SEO/SLLA blends collected in the melt state (T = 190 °C). The solid curves represent the fits of the experimental data by the paracrystalline model of lamellar structure considering polydispersity of lamellar thickness, limited grain size, and lattice distortion by thermal fluctuations. (b) Variations of the interlamellar distance (d) and the area per junction point at the lamellar interface (Σ) as a function of weight fraction of SLLA in the blends.

function of weight fraction of SLLA. The interfacial area per junction was obtained from[21]

$$\Sigma = 2\{[(1-n_{SLLA})N_{SEO,PS} + n_{SLLA}N_{SLLA,PS}]V_S + (1-n_{SLLA})N_{SEO,PEO}V_{EO} + n_{SLLA}N_{SLLA,PLLA}V_{LLA})/d\} \quad (1)$$

where n_j (j = SLLA or SEO) signifies the number fraction of the diblock copolymer in the blend, $N_{SEO,PS}$, $N_{SLLA,PS}$, $N_{SEO,PEO}$, and $N_{SLLA,PLLA}$ are the degrees of polymerization of PS, PEO, or PLLA blocks in SEO and SLLA, and V_i (with i = PS, PEO, or PLLA) is the volume of an i monomer unit (V_S = 0.164 nm^3, V_{EO} = 0.0652 nm^3, and V_{LLA} = 0.1013 nm^3).

The interlamellar distance was found to increase with increasing SLLA content, signaling that the PS blocks from the two copolymers and PEO and PLLA blocks mix intimately in their respective microdomains.[15−21] In this case, the longer PS and PLLA blocks from SLLA swelled PS and PEO/PLLA domains, respectively, causing an increase of d with increasing SLLA content. The cross-sectional area Σ, on the other hand, remained approximately constant at the value close to that in neat SEO. This behavior was in parallel with that found for the diblock blends exhibiting the cosurfactant effect.[20,21] In this case, each lamellar domain was constituted of two layers of brushes lying on top of each other. The first layer was formed by the shorter blocks and the first subchains in the longer blocks, while the second layer composed of the remaining subchains of the longer blocks.[21]

The miscibility between PEO and PLLA blocks was further evidenced by the depression of T_g from 58 °C for PLLA block in neat SLLA to ca. 28 °C on addition of 20 wt % of SEO (see Figure S1 of the Supporting Information). Our SAXS and DSC results have thus shown that the PS blocks from SEO and SLLA and the PEO and PLLA blocks were miscible in their respective microdomains. The blends exhibited a lamellar morphology consisting of alternating PS and PEO/PLLA lamellae in the melt state.

Crystallization Behavior of PEO and PLLA Blocks within Lamellar Microdomains. Over the T_c range investigated, the lamellar structure in the melt state was found to be preserved after the crystallization, as the SAXS profiles were essentially unperturbed. Therefore, the crystallizations of PLLA and PEO blocks were effectively confined within the lamellar microdomains. In this study, the crystallization behavior of PEO and PLLA blocks was investigated by the combination of temperature-dependent WAXS and DSC. Figure 2 displays a series of temperature-dependent WAXS profiles of SEO/SLLA blends having been isothermally crystallized at 30 °C (the corresponding results of neat SEO and SLLA can be found in Figure S3 of the Supporting Information). For the WAXS measurement, the sample was held at the prescribed temperature for 5 min followed by data acquisition for another 5 min for each measurement; thus, the time period for structural formation or reorganization at each temperature was 10 min.

Crystalline PEO is known to exhibit two strong reflections at 2θ = 19.05° and 23.17°, corresponding to (120) and (hkl) plane with d-spacing of 0.39 nm (at least seven (hkl) planes have similar d-spacing),[34,35] respectively (see Figure S2 of the Supporting Information). PLLA homopolymer was amorphous upon quenching from 190 to 30 °C, but the crystallinity developed significantly on subsequent heating to 60 °C, which was right above its T_g of 56 °C (see Figure S2 of the Supporting Information). In this case, two strong reflections at 2θ = 16.30° and 18.57° corresponding to (200)/(110) and (203) planes, respectively, of α-form crystal emerged.[36−38]

As shown in Figure 2a,b (and Figure S3 for SEO and SLLA), the characteristic reflections associated with PEO and PLLA crystals were observed once these two blocks exhibited reasonably high levels of crystallinity. This demonstrates that PEO and PLLA crystallites with identical crystallographic structure formed in the lamellar microdomains in the blends as those of the corresponding homopolymers. It is interesting that under the prescribed heating protocol the crystallization of PLLA block in quenched SLLA and blends occurred on heating to 100 °C, which is about the T_g of PS block. This indicates that the chain mobility associated with the cold crystallization of PLLA block was retarded by the junction points of the vitrified PS block. However, this does not mean that the crystallization of PLLA block in the PEO/PLLA blend domain was completely hindered when the PS domain remained vitrified (i.e., at $T_c < T_g^{PS}$). It will be shown later specifically for SLLA-rich blend that, as long as the annealing time was sufficiently long (e.g., 48 h), the α-form crystal of PLLA block could still develop significantly at T_cs < 100 °C.

Let us examine the temperature-dependent WAXS profiles of crystalline SEO-rich SEO/SLLA 80/20 blend (Figure 2a) in further detail. At this blend composition, the PEO fraction dominated in the PEO/PLLA lamellar microdomains and the T_g of the PEO/PLLA domain was ca. −44 °C as estimated from the Fox equation. Clearly, annealing at 30 °C was able to induce PEO crystallization as evidenced by the presence of PEO crystalline reflections in the WAXS profile at 30 °C, but the

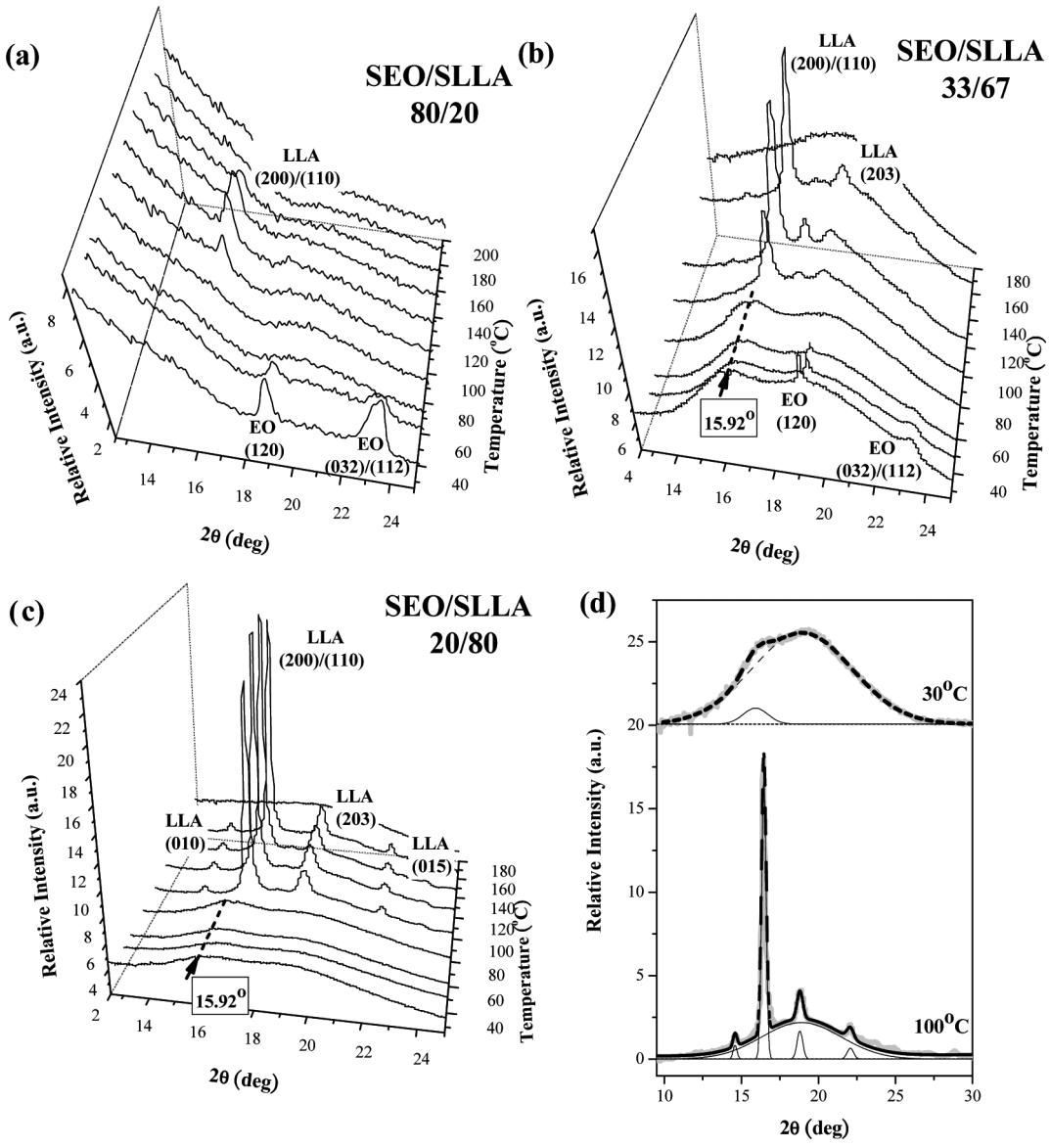

Figure 2. Temperature-dependent WAXS profiles of SEO/SLLA (a) 80/20, (b) 33/67, and (c) 20/80 blend collected after the samples have been isothermally annealed at 30 °C for 48 h. For 33/67 and 20/80 blends, a peculiar broad peak at $2\theta = 15.92°$ was observed at the as-crystallized state. This peak vanished and was replaced by the sharp (200)/(110) peak of PLLA crystals upon heating to 100 °C due to the occurrence of significant crystallization. (d) Deconvolution of the WAXS profiles of 20/80 blend observed at 30 and 100 °C into the constituting scattering peaks.

crystallinity of PLLA was negligible. The PEO crystalline peaks vanished upon heating to 60 °C ($T_m^{PEO} \approx 53$ °C) due to complete melting of PEO crystals. The characteristic PLLA crystalline reflection at $2\theta = 16.32°$ emerged on further heating to 100 °C and finally vanished at 180 °C ($> T_m^{PLLA} \approx 165$ °C). In this system, the crystallization of PEO blocks took place upon cooling to 30 °C due to higher concentration and high chain mobility ($T_c \gg T_g$); the PEO crystallinity attained was however lower than that in the corresponding homopolymer blend because the immobility of the junction points (due to vitrification of PS domain) localized at the lamellar interface limited the distance over which the PLLA chains could be expelled out of the crystal growth front during PEO crystallization. As a result, the crystal growth of PEO was "poisoned" by the surrounding PLLA blocks.[36] The crystallization of PLLA block at 30 °C was hampered completely by such a poisoning effect. However, when the temperature was raised to ca. 100 °C, the gain of junction point mobility of glassy PS layers and the enhancement of chain mobility allowed PLLA to crystallize to a detectable level of crystallinity under the prescribed heating protocol.

For the SLLA-rich 33/67 and 20/80 blends, a peculiar broad peak at $2\theta = 15.92°$ (corresponding to *d*-spacing of 5.56 Å) was observed at the as-crystallized state ($T_c = 30$ °C) (Figure 2b,c). This peak was not identified in the corresponding blends of PEO and PLLA homopolymers, and it vanished and was replaced by the sharp (200)/(110) peak of PLLA α-form crystals upon heating to ca. 100 °C due to the occurrence of significant crystallization. The observed WAXS profiles of 20/80 blend at 30 and 100 °C were further deconvoluted into the constituting scattering peaks, as shown in Figure 2d. At 30 °C the scattering curve contained a large amorphous halo at $2\theta = 18.82°$and a small peak at 15.92°. The relative areas of these two peaks prescribed the amounts of the two phases to be 95.85% and 4.15%, respectively. When the sample was heated to 100 °C, distinct PLLA crystalline peaks developed with the relative area of 34.62% and the scattering peak at 15.92° was not discernible.

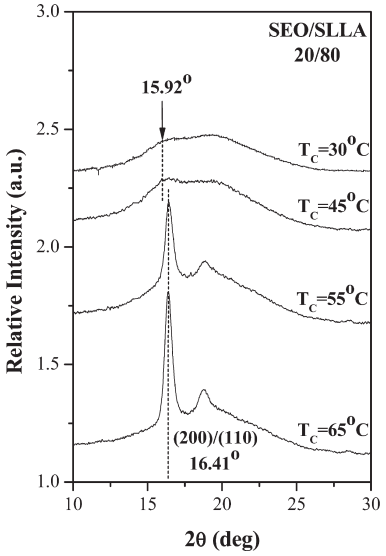

Figure 3. Room-temperature WAXS profiles of SEO/SLLA 20/80 blend having been crystallized at various T_cs for 48 h. It can be seen that the 15.92° peak was identified for T_c = 30 and 45 °C, while at $T_c \geq$ 55 °C significant crystallization of PLLA took place, giving rise to the sharp (200)/(110) peak at 2θ = 16.41°.

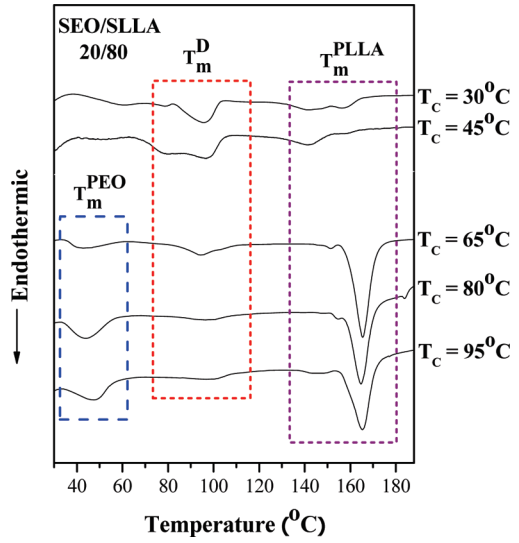

Figure 4. (a) DSC heating scans of SEO/SLLA 20/80 blend after isothermal crystallization at different T_cs for 48 h. The peculiar structure exhibited two melting peaks for T_cs lying below 65 °C, whereas only a single melting endotherm was identified when $T_c \geq$ 65 °C. Moreover, the melting peak of the peculiar structure progressively diminished with increasing T_c because the formal crystallization of PLLA blocks set in due to the enhancement of chain mobility.

The peculiar peak at 15.92° was found to develop in SLLA-rich copolymer blends only when the isothermal crystallization temperature was sufficiently low, as demonstrated by Figure 3 showing the room-temperature WAXS profiles of 20/80 blend having been crystallized at various T_cs values ranging from 30 to 65 °C. For this experiment, the blend was first annealed at 190 °C for 10 min to erase previous crystallization history followed by rapid cooling to the prescribed T_c for crystallization for 48 h. The WAXS profile of the sample thus crystallized was then collected at room temperature. It can be seen that the 15.92° peak was identified for T_c = 30 and 45 °C, while at $T_c \geq$ 55 °C significant crystallization of PLLA took place upon 48 h annealing even though the temperatures were still lower than T_g^{PS}.

The DSC experiment was conducted to examine the thermodynamic stability of the peculiar structure. Figure 4 displays the DSC heating scans of SEO/SLLA 20/80 blend subjecting to the same crystallization history as that of the samples used for obtaining the WAXS results in Figure 3. After the crystallization at the prescribed T_cs for 48 h, the samples were cooled to −5 °C at which the DSC scans started with the heating rate of 20 °C/min. In this case, PEO blocks were able to crystallize during the cooling, such that PEO melting endotherm appeared in the DSC thermograms in Figure 4. It can be seen that small endotherm(s) (marked by "T_m^D") was discernible at about 100 °C, besides the melting endotherms associated with PEO and PLLA α-form crystals located at ca. 50 and 145−165 °C, respectively. We consider these additional endotherms to be associated with the melting of the peculiar structure that gave rise to the broad WAXS peak at 2θ = 15.92°. The fact this peculiar structure melted at ca. 100 °C explained why the 15.92° peak vanished at 100 °C in the temperature-dependent WAXS profiles in Figure 2b,c. Moreover, this peculiar structure should be contributed primarily by PLLA blocks because its melting temperature was higher than T_m^{PEO} and it appeared in the blends with high SLLA composition.

It is further noted that the peculiar structure exhibited two melting peaks for T_cs lying below 65 °C, whereas only a single melting endotherm was identified when $T_c \geq$ 65 °C. The T_c dependence of the melting curve was in parallel with that of the conventional crystalline polymers displaying double melting peaks,[39,40] thereby implying that the peculiar structure should be crystalline in nature. Another interesting feature noted from Figure 4 is that the melting peaks of both PEO and PLLA α-form crystals showed up clearly for $T_c \geq$ 65 °C, whereas the melting peak of the peculiar structure was hardly discernible. On the other hand, the crystallinities of both PEO and PLLA were very low (or even undetectable for PEO) for the T_cs (= 30 and 45 °C) at which the peculiar structure clearly formed.

The DSC and WAXS results revealed that under the prescribed isothermal crystallization conditions (i.e., rapid cooling from 190 °C to the prescribed T_cs for crystallization for 48 h), the peculiar structure in SLLA-rich blends developed only at sufficiently low T_c ($T_g^{EO/LLA} \approx 28$ °C < $T_c \leq \sim 45$ °C). This peculiar structure was able to sustain up to ca. 100 °C as evidenced by the DSC scans in Figure 4. Significant crystallization of PLLA was able to take place at $T_c \geq \sim 55$ °C after the 48 h annealing. Therefore, the temperature range over which the peculiar structure may form was narrow. We postulated that the formation of the peculiar structure at low T_c and the occurrence of significant crystallization above ca. 55 °C were related to the chain mobility of PLLA block in the PEO/PLLA microdomains. The mobility term associated with the crystallization rate of a polymer is often expressed as $\exp[-U^*/R(T_c - T_0)]$, where U^* is the activation energy associated with the transport of chain segments to the crystal growth front and T_0 is the temperature at which such a transport ceases. Using the classical values of U^* = 1500 cal/mol and $T_0 = T_g^{EO/LLA} - 30$,[41] we found that the T_c at which the value of the mobility term starts to increase abruptly was close to 55 °C (see Figure S4 of the Supporting Information). This hence suggests that the chain mobility associated with the crystallization of PLLA was highly restricted below 55 °C, whereas such a restriction was obviously released above this temperature.

Consequently, the proposed structural development in SLLA-rich blends proposed in Figure 5. At sufficiently high T_c ($\geq\sim$55 °C), both PEO and PLLA blocks had higher chain mobility; therefore, the formal crystallization involving rather long-range transport of PLLA chains to the crystal

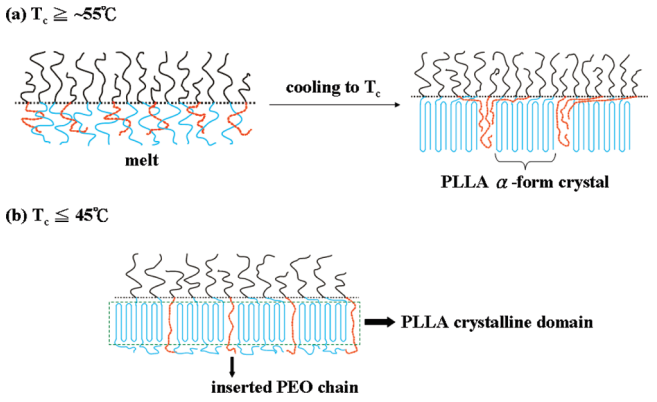

Figure 5. Schematic illustration of the structural development in SLLA-rich blends. (a) At sufficiently high T_c (≥55 °C), the formal crystallization involving rather long-range transport of PLLA chains to the crystal growth front could take place more easily. The amorphous PEO blocks segregated locally during the PLLA crystallization underwent crystallization upon cooling to below T_m^{PEO}. (b) At low T_c (≤45 °C), the formal crystallization was strongly hampered; however, a local demixing between PEO and PLLA chains took place to yield PLLA crystalline domains in which the crystalline stems were intervened by PEO chains.

growth front could take place more easily even if the junction points were fixed at the vitrified PS domain interface, leading to relatively high PLLA crystallinity (as illustrated in Figure 5a), and the PLLA crystallites thus generated exhibited a melting point at ca. 165 °C. During the PLLA crystallization, amorphous PEO blocks were segregated locally (under the influence of the junction point constraint), such that the concentration of PEO in the amorphous regions surrounding the PLLA crystallites became higher than the initial concentration. When the blend was cooled to below T_m^{PEO}, PEO blocks crystallized from these amorphous regions, generating PEO crystallites.

On the other hand, at low T_c (≤~45 °C) the formal crystallization of PLLA was strongly hampered by the highly restricted chain mobility of PLLA and junction point constraint. However, we propose that a local demixing between a fraction of PEO and PLLA chains could still take place to yield PLLA crystalline domains in which the PLLA crystalline stems were intervened by the PEO chains (see Figure 5b). It is speculated that the presence of the inserted PEO chains served as the molecular (line) defects and induced an expansion of the *a*-axis and *b*-axis of the α-form PLLA unit cell (so as to shift the (200)/(110) peak to 15.92°) while the *c*-axis along the chain direction remained unchanged.[42,43] The excess free energy associated with these defects caused a significant depression of melting point to ca. 100 °C.

Orientation of PLLA Crystallites in the Lamellar Microdomains. We have also examined the crystal orientation of PLLA in 20/80 blend. In this case, the oriented crystalline blend was prepared by LAOS at 190 °C followed by rapid quench to the desired T_c for crystallization. Figure 6a−c shows the 2-D SAXS patterns viewed along the tangential, radial, and normal directions (designated as *x*, *y*, and *z*, respectively). The presence of arcs in the 2-D SAXS patterns indicates that large-scale orientations of the microdomains were accomplished by LAOS. The SAXS patterns were almost identical along *x* and *y* directions and the fact that the diffraction arcs were located at the meridians indicated that the lamellar microdomains stacked along the *z* direction. By contrast, only a weak isotropic pattern was observed in the 2-D pattern along the *z* direction. This suggests that lamellar microdomains adopt random orientation when the X-ray is directed along the layer normal direction.

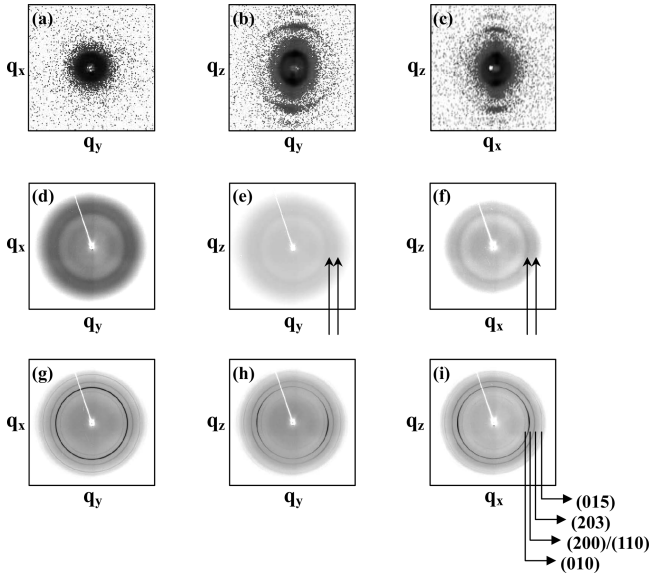

Figure 6. (a−c) 2-D SAXS patterns viewed along the tangential, radial and normal directions (designated as *x*, *y*, and *z*, respectively) of sheared-aligned 20/80 blend. 2-D patterns indicate that the lamellar microdomains stacked along the *z* direction. (d−f) 2-D WAXS patterns along *z*, *x*, and *y* direction of the blend having been crystallized at 30 °C. The defective crystalline domains exhibited a pair of arcs (marked by the arrows) in the equator in the tangential and radial views. (g−i) 2-D WAXS patterns of 20/80 blend having been crystallized at 100 °C. Four PLLA diffractions, i.e., (010), (200)/(110), (203), and (015), appeared clearly. The feature of the 2-D patterns indicates that the crystalline stems of PLLA aligned normal to the lamellar interface.

Figure 6d−f displays the corresponding 2-D WAXS patterns along *z*, *x*, and *y* direction, respectively, of the blend having been crystallized at 30 °C. The defective crystalline domains contributed predominately to the crystalline phase in this sample. It can be seen that these domains exhibited a pair of arcs in the equator in the tangential and radial views, while only an isotropic ring was observed in the normal view. This indicates that the crystalline domains were highly oriented when viewed along *x* and *y* directions, but the orientation was rather random when looking through the *z* direction (i.e., the system displayed the in-plane orientation).

With the occurrence of appreciable crystallization of PLLA block at higher T_cs, the strong diffractions of PLLA crystals became discernible in the 2-D WAXS patterns. Figure 6g−i shows the 2-D WAXS patterns of 20/80 blend having been crystallized at 100 °C. Four PLLA diffractions, i.e., (010), (200)/(110), (203), and (015), appeared clearly. For the tangential and radial views, it can be seen that the (200) arcs appeared at the equator, meaning that the crystalline stems of PLLA aligned normal to the lamellar interface. Such a homeotropic orientation was prevalent among crystalline diblock copolymers[44−48] and has been observed in other PLLA-based diblock systems.[49]

Conclusions

We have studied the morphology and crystallization behavior of the binary blends of a PS-*b*-PEO and a PS-*b*-PLLA. In the melt state the PS blocks from these two copolymers mixed intimately in the PS lamellar microdomains and PEO and PLLA blocks also formed a miscible mixture in their mcrodomains. The lamellar structure formed in the melt state was effectively preserved upon crystallization of PEO and PLLA blocks. Because of the intimate mixing and the junction point constraint, the crystallization behavior of PLLA block in SLLA-rich blends was significantly modified comparing to that in the corresponding homopolymer blends. At sufficiently low

T_c (≤45 °C), the formal crystallization was strongly hampered by the restricted chain mobility of PLLA coupled with the junction point constraint; however, a local demixing between a fraction of PEO and PLLA chains occurred to generate the PLLA crystalline domains in which the crystalline stems were intervened by PEO chains. These domains exhibited a melting point of ca. 100 °C and gave rise to a peak at $2\theta = 15.92°$ in the WAXS profile. Finally, using the macroscopically oriented 20/80 blend, the PLLA stems in the crystallites within the lamellar microdomains at $T_c = 100$ °C were found to orient normal to the lamellar interface.

Acknowledgment. We gratefully acknowledge financial support from the National Science Council Taiwan under Contract NSC 95-2221-E-007-083.

Supporting Information Available: Glass transition regions in the DSC thermograms of SLLA and SEO/SLLA 33/67 and 20/80 blends; temperature-dependent WAXS profiles of PEO and PLLA homopolymers; temperature-dependent WAXS profiles of neat SEO and SLLA; T_c dependence of the mobility term associated with the crystallization rate of SEO/SLLA 20/80 blend. This material is available free of charge via the Internet at http://pubs.acs.org.

References and Notes

(1) Loo, Y.-L.; Register, R. A. *Developments in Block Copolymer Science and Technology*; Hamley, I. W., Ed.; Wiley: New York, 2004; Chapter 6.
(2) Müller, A. J.; Balsamo, V.; Arnal, M. L. *Adv. Polym. Sci.* **2005**, *190*, 1.
(3) Reiter, G.; Castelein, G.; Sommer, J.-U. In *Polymer Crystallization: Observations, Concepts and Interpretations*; Sommer, J.-U., Reiter, G., Eds.; Springer: Berlin, 2003; Chapter 8.
(4) Huang, P.; Zhu, L.; Guo, Y.; Ge, Q.; Jing, A. J.; Chen, W. Y.; Quirk, R. P.; Cheng, S. Z. D.; Thomas, E. L.; Lotz, B.; Hsiao, B. S.; Avila- Orta, C. A.; Sics, I. *Macromolecules* **2004**, *37*, 3689.
(5) Zhu, L.; Cheng, S. Z. D.; Calhoun, B. H.; Ge, Q.; Quirk, R. P.; Thomas, E. L.; Hsiao, B. S.; Yeh, F.; Lotz, B. *J. Am. Chem. Soc.* **2000**, *122*, 5957.
(6) Hamley, I. W.; Fairclough, J. P. A.; Terrill, N. J.; Ryan, A. J.; Lipic, P. M.; Bates, F. S.; Towns-Andrews, E. *Macromolecules* **1996**, *29*, 8835.
(7) Quiram, D. J.; Register, R. A.; Marchand, G. R. *Macromolecules* **1997**, *30*, 4551.
(8) Quiram, D. J.; Register, R. A.; Marchand, G. R.; Ryan, A. J. *Macromolecules* **1997**, *30*, 8338.
(9) Quiram, D. J.; Register, R. A.; Marchand, G. R.; Adamson, D. H. *Macromolecules* **1998**, *31*, 4891.
(10) Hsiao, M.-S.; Zheng, J. X.; Leng, S. W.; Van Horn, R. M.; Quirk, R. P.; Thomas, E. L.; Chen, H.-L.; Hsiao, B. S.; Rong, L.; Lotz, B.; Cheng, S. Z. D. *Macromolecules* **2008**, *41*, 8114.
(11) Huang, P.; Zhu, L.; Cheng, S. Z. D.; Ge, Q.; Quirk, R. P.; Thomas, E. L.; Lotz, B.; Hsiao, B. S.; Liu, L.; Yeh, F. *Macromolecules* **2001**, *34*, 6649.
(12) Nojima, S.; Tanaka, H.; Rohadi, A.; Sasaki, S. *Polymer* **1998**, *39*, 1727.
(13) Zhu, L.; Chen, Y.; Zhang, A.; Calhoun, B. H.; Chun, M.; Quirk, R. P.; Cheng, S. Z. D.; Hsiao, B. S.; Yen, F.; Hashimoto, T. *Phys. Rev. B* **1999**, *60*, 10022.
(14) Zhu, L.; Cheng, S. Z. D.; Calhoun, B. H.; Ge, Q.; Quirk, R. P.; Thomas, E. L.; Hsiao, B. S.; Yen, F.; Lotz, B. *Polymer* **2001**, *42*, 5829.
(15) Hashimoto, T.; Yamasaki, K.; Koizumi, S.; Hasegawa, H. *Macromolecules* **1993**, *26*, 2895.
(16) Mayes, A. M.; Russell, T. P.; Deline, V. R.; Satija, S. K.; Majkrzak, C. F. *Macromolecules* **1994**, *27*, 7447.
(17) Yamaguchi, D.; Hashimoto, T. *Macromolecules* **2001**, *34*, 6495.
(18) Shi, A. C.; Noolandi, J. *Macromolecules* **1994**, *27*, 2936.
(19) Shi, A. C.; Noolandi, J.; Hoffmann, H. *Macromolecules* **1994**, *27*, 6661.
(20) Court, F.; Hashimoto, T. *Macromolecules* **2001**, *34*, 2536.
(21) Court, F.; Hashimoto, T. *Macromolecules* **2002**, *35*, 2566.
(22) Huang, Y. Y.; Nandan, B.; Chen, H. L.; Liao, C. S.; Jeng, U. S. *Macromolecules* **2004**, *37*, 8175.
(23) Younes, H.; Cohn, D. *Eur. Polym. J.* **1988**, *24*, 765.
(24) Nakafuku, C.; Sakoda, M. *Polym. J.* **1993**, *25*, 909.
(25) Nakafuku, C. *Polym. J.* **1996**, *28*, 568.
(26) Nijenhuis, A. J.; Pennings, A. J. *Polymer* **1996**, *37*, 5849.
(27) Yang, J. M.; Chen, H. L.; You, J. W.; Hwang, J. C. *Polym. J.* **1997**, *8*, 657.
(28) Lai, W. C.; Liau, W. B.; Lin, T. T. *Polymer* **2004**, *45*, 3073.
(29) Mao, H.; Hillmyer, M. A. *Macromol. Chem. Phys.* **2008**, *209*, 1647.
(30) Mao, H.; Arrechea, P. L.; Bailey, T. S.; Johnson, B. J. S.; Hillmyer, M. A. *Faraday Discuss.* **2005**, *128*, 149.
(31) Mao, H.; Hillmyer, M. A. *Soft Matter* **2006**, *2*, 57.
(32) Förster, S.; Timmann, A.; Schellbah, C.; Meyer, A.; Funari, S. S.; Mulvaney, P.; Knott, R. *J. Phys. Chem. B* **2005**, *109*, 1347.
(33) Zalusky, A. S.; Olayo-Valles, R.; Wolf, J. H.; Hillmyer, M. A. *J. Am. Chem. Soc.* **2002**, *124*, 12767.
(34) Cheng, S. Z. D.; Wu, S. S.; Chen, J.; Zhuo, Q.; Quirk, R. P.; von Meerwall, E. D.; Hsiao, B. S.; Habenschuss, A.; Zschack, P. R. *Macromolecules* **1993**, *26*, 5105.
(35) Takahashi, Y.; Tadokoro, H. *Macromolecules* **1973**, *6*, 672.
(36) Ungar, G.; Putra, E. G. R.; de Silva, D. S. M.; Shcherbina, M. A.; Waddon, A. J. *Adv. Polym. Sci.* **2005**, *180*, 45.
(37) Cho, J.; Baratian, S.; Kim, J.; Yeh, F.; Hsiao, B. S.; Runt, J. *Polymer* **2003**, *44*, 711.
(38) Mano, J. F.; Wang, Y.; Viana, J. C.; Denchev, Z.; Oliveira, M. J. *Macromol. Mater. Eng.* **2004**, *289*, 910.
(39) Yoo, E. S.; Im, S. S. *J. Polym. Sci., Polym. Phys.* **1999**, *37*, 1357.
(40) Qiu, Z.; Ikehara, T.; Nishi, T. *Polymer* **2003**, *44*, 2799.
(41) Hoffman, J. D.; Davis, G. T.; Lauritzen, J. I. In *Treatise on Solid State Chemistry*; Hannay, N. B., Ed.; Plenum: New York, 1976; Vol. *3*, Chapter 7.
(42) Preedy, J. E. *Br. Polym. J.* **1973**, *5*, 13.
(43) Martinez-Salazar, F. J.; Balta'-Calleja, F. J. *J. Cryst. Growth* **1979**, *48*, 282.
(44) Lotz, B.; Kovacs, A. J. *Kolloid Z. Z. Polym.* **1966**, *209*, 97.
(45) Lotz, B.; Kovacs, A. J.; Bassett, G. A.; Keller, A. *Kolloid Z. Z. Polym.* **1966**, *209*, 115.
(46) Kovacs, A. J.; Lotz, B.; Keller, A. *J. Macromol. Sci. Phys.* **1969**, *B3*, 385.
(47) Hirata, E.; Ijitsu, T.; Hashimoto, T.; Kawai, H. *Polymer* **1975**, *16*, 249.
(48) Yang, Y. W.; Tanodekaew, S.; Mai, S. M.; Booth, C.; Ryan, A. J.; Bras, W.; Viras, K. *Macromolecules* **1995**, *28*, 6029.
(49) Ho, R. M.; Lin, F. H.; Tsai, C. C.; Lin, C. C.; Ko, B. T.; Hsiao, B. S.; Sics, I. *Macromolecules* **2004**, *37*, 5985.